Dual-pump parametric amplification in dispersion engineered photonic crystal waveguides

A. Willinger,[1,*] S. Roy,[2,3] M. Santagiustina,[2] S. Combrié,[4] A. De Rossi,[4] I. Cestier,[1] and G. Eisenstein[1]

[1]*Electrical Engineering Department, Technion Israel Institute of Technology, Technion City, Haifa, 32000, Israel*
[2]*CNIT, Dipartimento di Ingegneria dell'Informazione, Università di Padova, via Gradenigo 6b, Padova, 35131, Italy*
[3]*Department of Physics, National Institute of Technology, Warangal, 506004, India*
[4]*Thales Research and Technology, Route Départementale 128, 91767, Palaiseau, France*

[*]*amnon.willinger@gmail.com*

Abstract: This paper describes a numerical simulation of narrow band parametric amplification in dispersion engineered photonic crystal waveguides. The waveguides we analyze exhibit group velocity dispersion functions which cross zero twice thereby enabling many interesting pumping schemes. We analyze the case of two pulsed pumps each placed near one of the zero dispersion wavelengths. These configurations are compared to conventional single pump schemes. The two pumps may induce phase matching conditions in the same spectral location enabling to control the gain spectrum. This is used to study the gain and fidelity of 40*Gbps* NRZ data signals.

© 2013 Optical Society of America

References

1. L. H. Frandsen, A. V. Lavrinenko, J. Fage-Pedersen, and P. I. Borel, "Photonic crystal waveguides with semi-slow light and tailored dispersion properties," Opt. Express **14**, 9444–9450 (2006).
2. J. W. Li, T. P. O'Faolain, L. Gomez-Iglesias, A. Krauss, and T. F, "Systematic design of flat band slow light in photonic crystal waveguides," Opt. Express **16**, 6227–6232 (2008).
3. Y. Hamachi, S. Kubo, and T. Baba, "Slow light with low dispersion and nonlinear enhancement in a lattice-shifted photonic crystal waveguide," Opt. Lett. **34**, 1072–1074 (2009).
4. M. Shinkawa, N. Ishikura, Y. Hama, K. Suzuki, and T. Baba, "Nonlinear enhancement in photonic crystal slow light waveguides fabricated using cmos-compatible process," Opt. Express **19**, 22208–22218 (2011).
5. N. A. R. Bhat and J. E. Sipe, "Optical pulse propagation in nonlinear photonic crystals," Phys. Rev. E **64**, 056604 (2001).
6. A. S. Y. Hseih, G. K. L. Wong, S. G. Murdoch, S. Coen, F. Vanholsbeeck, R. Leonhardt, and J. D. Harvey, "Combined effect of kerr and raman nonlinearities on single-pump optical parametric amplifiers," in *Proceedings of the 33rd European Conference and Ehxibition of Optical Communication* (Berlin, Germany, 2007) 1–2.
7. M. Santagiustina, C. G. Someda, G. Vadala, S. Combrié, and A. D. Rossi, "Theory of slow light enhanced four-wave mixing in photonic crystal waveguides," Opt. Express **18**, 21024–21029 (2010).
8. B. Corcoran, C. Monat, M. Pelusi, C. Grillet, T. P. White, L. OFaolain, T. F. Krauss, B. J. Eggleton, and D. J. Moss, "Optical signal processing on a silicon chip at 640Gb/s using slow-light," Opt. Express **18**, 7770–7781 (2010).
9. I. Cestier, A. Willinger, V. Eckhouse, G. Eisenstein, S. Combrié, P. Colman, G. Lehoucq, and A. D. Rossi, "Time domain switching / demultiplexing using four wave mixing in gainp photonic crystal waveguides," Opt. Express **19**, 6093–6099 (2011).

10. I. Cestier, S. Combrié, S. Xavier, G. Lehoucq, A. D. Rossi, and G. Eisenstein, "Chip-scale parametric amplifier with 11db gain at 1550nm based on a slow-light gainp photonic crystal waveguide," Opt. Lett. **37**, 3996–3998 (2012).
11. P. Colman, S. Combrié, G. Lehoucq, and A. De Rossi, "Control of dispersion in photonic crystal waveguides using group symmetry theory," Opt. Express **20**, 13108–13114 (2012).
12. S. Roy, M. Santagiustina, P. Colman, S. Combrié, and A. De Rossi, "Modeling the dispersion of the nonlinearity in slow mode photonic crystal waveguides," Photonics Journal **4**, 224–233 (2012).
13. S. Roy, A. Willinger, S. Combrié, A. D. Rossi, G. Eisenstein, and M. Santagiustina, "Narrowband optical parametric gain in slow mode engineered GaInP photonic crystal waveguides," Opt. Lett. **37**, 2919–2921 (2012).
14. A. Willinger, S. Roy, M. Santagiustina, S. Combrié, A. D. Rossi, I. Cestier, and G. Eisenstein, "Parametric gain in dispersion engineered photonic crystal waveguides," Opt. Express **21**, 4995–5004 (2013).
15. D. Dahan and G. Eisenstein, "Tunable all optical delay via slow and fast light propagation in a raman assisted fiber optical parametric amplifier: a route to all optical buffering," Opt. Express **13**, 6234–6249 (2005).
16. E. Shumakher, A. Willinger, R. Blit, D. Dahan, and G. Eisenstein, "Large tunable delay with low distortion of 10 gbit/s data in a slow light system based onnarrow band fiber parametric amplification," Opt. Express **14**, 8540–8545 (2006).
17. A. Willinger, E. Shumakher, and G. Eisenstein, "On the roles of polarization and raman-assisted phase matching in narrowband fiber parametric amplifiers," J. Lightwave Technol. **26**, 2260–2268 (2008).
18. A. Gershikov, E. Shumakher, A. Willinger, and G. Eisenstein, "Fiber parametric oscillator for the 2 μm wavelength range based on narrowband optical parametric amplification," Opt. Lett. **35**, 3198–3200 (2010).
19. G. Agrawal, *Nonlinear Fiber Optics* (Academic Press, 2001).
20. A. Willinger and G. Eisenstein, "Split step fourier transform: A comparison between single and multiple envelope formalisms," J. Lightwave Technol. **30**, 2988–2994 (2012).
21. O. Sinkin, R. Holzlohner, J. Zweck, and C. Menyuk, "Optimization of the split-step fourier method in modeling optical-fiber communications systems," J. Lightwave Technol. **21**, 61–68 (2003).
22. P. V. Mamyshev and S. V. Chernikov, "Ultrashort-pulse propagation in optical fibers," Opt. Lett. **15**, 1076–1078 (1990).
23. G. K. L. Wong, S. G. Murdoch, R. Leonhardt, J. D. Harvey, and V. Marie, "High-conversion-efficiency widely-tunable all-fiber optical parametric oscillator," Opt. Express **15**, 2947–2952 (2007).

1. Introduction

Major advancements in dispersion engineered photonic crystal (PhC) waveguides [1–4] have led to many new applications where slow mode propagation is exploited for the enhancement of nonlinear processes [5–7]. Examples include optical signal processing [8, 9] and efficient optical parametric amplification (OPA) [10] implemented in chip scale devices.

We address here a particular family of dispersion engineered PhC waveguides comprising a wide band gap GaInP PhC structure with air holes having a basic periodicity of 465nm. The 1.3mm long waveguide core is a defect line of removed holes, while the dispersion properties are determined by an asymmetric shift of the two innermost rows [11, 12]. The design yields dispersive field mode distributions leading to a dispersive linear group velocity (GVD) as well as frequency dependent losses and nonlinear coefficients of different wave mixing interactions. The latter is usually not addressed in propagation models of fiber based nonlinear devices, while here the effective nonlinear coefficient for self and cross phase modulation (SPM and XPM, respectively) and for four wave mixing (FWM) were modeled accurately [7, 12]. The GVD of these waveguides exhibits two zero dispersion wavelengths (ZDWs) with the dispersion in the spectral region between them being normal ($\beta_2 > 0$). Further analysis (which incorporated the effect of loss dispersion) [13] has shown the potential of these dispersion engineered PhC waveguides for narrowband OPA (NB-OPA) induced by a constant pump.

Figures 1(a) and 1(b) show the different propagation parameters for different engineered PhC waveguides which differ by their asymmetric shift parameter T [12]. In order to simulate the parametric processes, we describe the dispersion using at least fifteen orders of the $\beta(\omega)$ function. The effect on NB-OPA generated by a pulsed pump was recently explored [14]. Increasing T was shown to lead to a widening of the distance between the two ZDWs, to an increase in the SPM nonlinearity near the short ZDW, and also to a reduction of the FWM nonlinearity in

neighboring wavelengths. The characteristics of the NB-OPA change as T grows such that for a given pump wavelength, the signal-pump detuning range increases, the gain spectrum narrows and the maximum attainable gain is lowered.

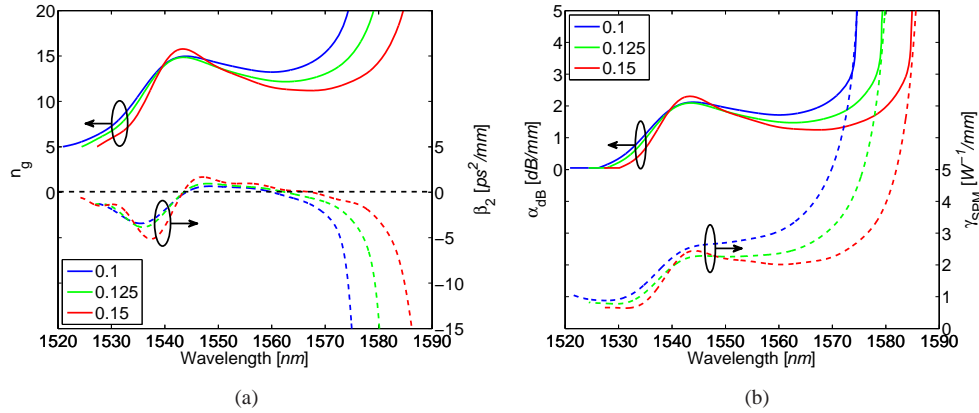

(a)   (b)

Fig. 1. Dispersion of the propagation parameters of the engineered PhC waveguides: (a) group index and GVD, (b) losses and SPM nonlinearity. The different curves represent different values of the ratio T/a: 0.1, 0.125 and 0.15.

NB-OPA in optical fibers is a well established process offering tunable filters and ampli-fiers [6, 15], slow and fast light devices [15–17] and tunable optical parametric oscillators (OPO) [18]. Down scaling to nano-structured PhC devices has several advantages in addition to the obvious size reduction and integration capabilities. The two ZDWs of the engineered PhC waveguides allow to combine two NB-OPA processes, induced by two separate pumps, each located near one ZDW. Such dispersion functions cannot be obtained in regular fibers, while in PhC fibers they are available in principle, but in practice, only very specific cases have been implemented. Operation with two pumps enhances the parametric gain for a signal tuned to the region of the narrowband gain. The two pump waves, termed hereon as the blue-pump (with shorter wavelength $\lambda_{p,b}$) and red-pump (with longer wavelength $\lambda_{p,r}$), can be launched into the waveguide in different configurations producing either larger gain or a wider gain spec-trum, thus supporting high bit-rate signals. Since FWM of two strong waves [19] produces idler waves by itself, a configuration may also be found where the two pumps are launched (without a signal to be amplified) and produce idler waves that are built up in phased-matched wavelength regions.

Throughout this article, we compute the propagation of strong pump waves with or without a signal and with many idler waves that are generated along the waveguide due to the FWM process. These could be constant waves (CW), pulses or NRZ modulated data streams. We use the M-SSFT algorithm [20] as the numerical computation method since it supports all forms of signal envelopes, losses and most important the dispersive nature of both linear and nonlinear propagation parameters. As was noted in previous works [7, 12, 14], the nonlinear parameter changes with wavelength and with the process at hand - SPM, XPM and FWM. Conventional SSFT [21] cannot support the dispersion of the nonlinearity and hence introduces unacceptable errors. Other numerical approaches as in [22] fail to solve the problem since they lose all their advantages when the field distribution varies significantly with wavelength as is the case in the present waveguides [12].

A discussion on FWM induced by two pumps is given in section 2, followed by a review of the simulation conditions (and limitations) in section 3. We then present simulation results

for two pulsed pumps and amplified idlers in section 4, and for an amplified pulsed signal by two pulsed pumps in section 5. The final scenario given in section 6 discusses the gain and distortion of a 40$Gbps$ NRZ data signal using two CW pumps.

2. FWM induced by two pumps

Two-pump FWM in optical fibers is a well documented process [19] in which two pump photons at frequencies $\omega_{p,b}$ and $\omega_{p,r}$ (referred to hereon as the blue-pump and red-pump, respectively) are transformed into two photons at the signal and idler frequencies ω_s and ω_i, respectively, such that $\omega_{p,b} + \omega_{p,r} = \omega_s + \omega_i$. The optical spectrum is schematically described in Fig. 2(a). Momentum conservation requires that the two pumps and their mixing products be phased matched, namely $\Delta k = \beta_s + \beta_i - \beta_{p,b} - \beta_{p,r}$ should approach zero. In optical fibers having conventional dispersion profiles (characterized by a single ZDW), phase matching can be obtained for all four waves, while the simultaneous degenerate FWM process of three waves is suppressed because of a phase miss-match.

   In the cases we analyze, which is schematically described in Fig. 2(b), degenerate FWM is an important process, however. Two photons from the blue pump and two from the red pump are converted into two photons of the desired signal at ω_s and two more photons at the appropriate idler frequencies $\omega_{i,b}$ and $\omega_{i,r}$, such that $2\omega_{p,b} = \omega_s + \omega_{i,b}$ and $2\omega_{p,r} = \omega_s + \omega_{i,r}$. Phase matching requires that $\Delta k_b = \beta_s + \beta_{i,b} - 2\beta_{p,b}$ and $\Delta k_r = \beta_s + \beta_{i,r} - 2\beta_{p,r}$ approach zero. While this seems improbable to maintain in conventional optical fibers, the complex dispersion function of the engineered PhC waveguides allows it and different corresponding scenarios are discussed in the following sections.
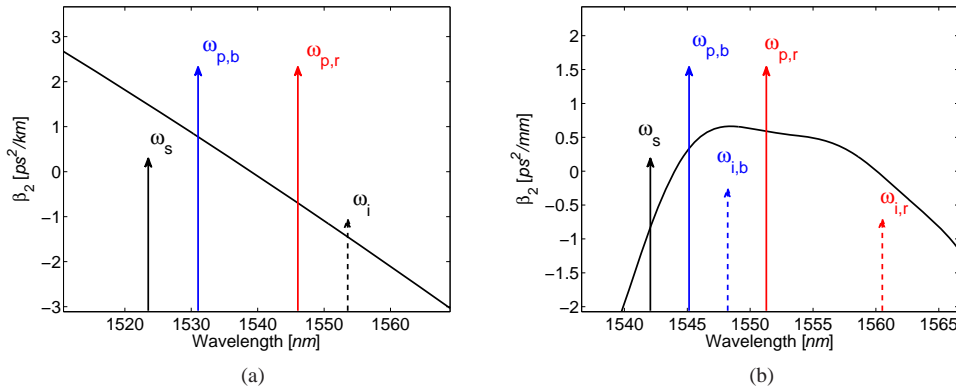

(a)　　　　　　　　　　　　　　　(b)

Fig. 2. Schematic description of FWM with two pumps (blue and red arrows) and a signal wave (black arrow) in (a) a dispersion shifted fiber, and (b) a dispersion engineered PhC. Exemplary spectra of the dispersion coefficient β_2 are shown in black curves for each waveguide type. The idlers in (b) match the pump with which they are phased matched.

   It is also notable that there are many degrees of freedom in choosing the signal wavelength in respect to the pump wavelengths. In this work we focus mainly on the case where the desired amplified signal is at shorter wavelengths than that of both pumps, however it is possible with these complex dispersion functions to have the signal placed in between the two pumps, equally detuned from each of them. A discussion on the limitations and degrees of freedom in choosing

the signal and pump wavelengths is given in section 3.

For the case of two pumps and no signal, the parametric process comprises wave mixing between the pumps. The two pumps that are detuned by $\Delta\Omega_p = \omega_{p,b} - \omega_{p,r}$ generate two idlers at lower and higher frequencies $\omega_{i,r}$ and $\omega_{i,b}$, which are detuned by the same amount $\Delta\Omega_p$ from each pump respectively. Phase matching condition is not optimal for the four waves together, yet the selection of the blue and red pump wavelengths with respect to the complex dispersion profiles ensures that phase matching is satisfied for two groups of degenerate FWM processes. The most dominant parametric process involves the two pumps and the idler at $\omega_{i,b}$; nevertheless, phase matching is also satisfied between this idler at ω_{ib}, the red pump at $\omega_{p,r}$ and an idler of higher order which is doubly detuned at $\omega_{p,r} - 2\Delta\Omega_p$. The blue pump transfers energy to the idler at $\omega_{i,b}$ and to the red pump which transfers in turn transfers energy to the same idler and to another high-order idler.

3. Simulation conditions

The propagation of two strong pumps and a signal wave under phase matched conditions generates many idler waves; some formed by the two pumps beating with each other and others resulting from FWM interactions between the signal and either of the pumps or their idlers. Referring to the propagation model in [20], the FWM contribution to the mth envelope is given by

$$\sum_{\{a,b,c\}} \gamma_{a,b,c,m} A_a A_b A_c^* \exp\left(j\Delta k_{abcd} \cdot z\right), \tag{1}$$

where the summation includes all the mixing terms for any combination of waves $\{a,b,c\}$ such that their carrier frequencies comply with

$$\omega_a + \omega_b = \omega_c + \omega_m, \tag{2}$$

and their propagation coefficients set the phase mismatch $\Delta k_{abcm} = \beta_a + \beta_b - \beta_c - \beta_m$. These conditions are satisfied by many combinations as seen in the exemplary spectrum shown in Fig. 3(a), where several idlers are maintained between the signal and the pumps. When using the M-SSFT algorithm, we account not only for the two pumps, the signal and the idler at $\tilde{\omega}_i = \omega_{p,b} + \omega_{p,r} - \omega_s$, but also for all idlers whose carrier frequencies comply with Eq. (2) together with either pump, the signal or other idlers. All idlers other than the one at $\tilde{\omega}_i$, are termed hereon high-order idlers (not to be confused with high-order nonlinearity which is not addressed in this work). The output spectrum in Fig. 3(a) shows that it is not possible to predict which of the high-order idlers can be neglected and hence they are all accounted for as long as they are within the waveguide transmission band.

As mentioned earlier, the use of the M-SSFT algorithm is necessary in order to account for the dispersion of the nonlinear parameters [13, 14], yet it also sets a limitation on the wavelengths of the three input waves. Given a set of envelope channels each with spectral width F_s (defined by the sampling frequency), two neighboring waves cannot be detuned from each other by less than F_s (otherwise the use of M-SSFT is not valid [20]). An arbitrary choice of wavelengths for the two pumps and the signal can lead to numerous FWM products $\{a,b,c,m\}$ including many high-order idlers that might be separated by less than F_s from neighboring signal, pump or idler waves. The spectrum in Fig. 3(a) represents a specific choice of wavelengths for the signal and two pumps, such that there is a finite number of FWM products $\{a,b,c,m\}$ and all possible waves are not separated by less than the chosen F_s. This is possible when the detuning of the signal from the closest pump complies with

$$\omega_s - \omega_{p,b} = q\Omega_p \equiv \left(p + \frac{m}{n}\right)(\omega_{p,b} - \omega_{p,r}), \tag{3}$$

where q is a rational number, and p, m and n are integers such that $n > m \geq 0$ and $p \geq 0$. With this selection of carrier frequencies, the detuning between two neighboring channels is

$$\Delta\omega_{min} = \begin{cases} \frac{\Omega_p}{n} & ,m > 0 \\ \Omega_p & ,m = 0, n = 1 \end{cases}. \tag{4}$$

This channel separation is maintained as long as $2\pi n F_s \leq \Omega_p$.

Even with this limitation on the frequencies of the waves, there are several degrees of freedom in the simulation conditions and the choice of inputs. We further narrow them according to the phase matching conditions among the input waves. We use the same expression for the parametric gain coefficient as in Eq. (1) of [14] and construct a FWM map (which exhibits regions where the gain coefficient is real) for a single pump as seen in Fig. 3(b). Using this map, we identify pairs of pump wavelengths, each in the vicinity of a different ZDW, for which phase matching is satisfied at the same signal wavelength. The dashed lines in Fig. 3(b) mark such a possible combination of pumps. We refer to such a couple of pumps as a dual-pump scheme. Together with the condition imposed by q, the choice of input pumps and signal is performed as follows: (1) set the blue-pump wavelength in the normal dispersion region, near the short ZDW; (2) select a q value and a sampling frequency F_s; (3) tune over a range of signal wavelengths for which a dual-pump scheme that includes the selected blue-pump is valid; (4) for each signal wavelength and blue-pump we set the red-pump according to Eq. (3), such that

$$\omega_{p,r} = \frac{(1+q)\omega_{p,b} - \omega_s}{q}. \tag{5}$$
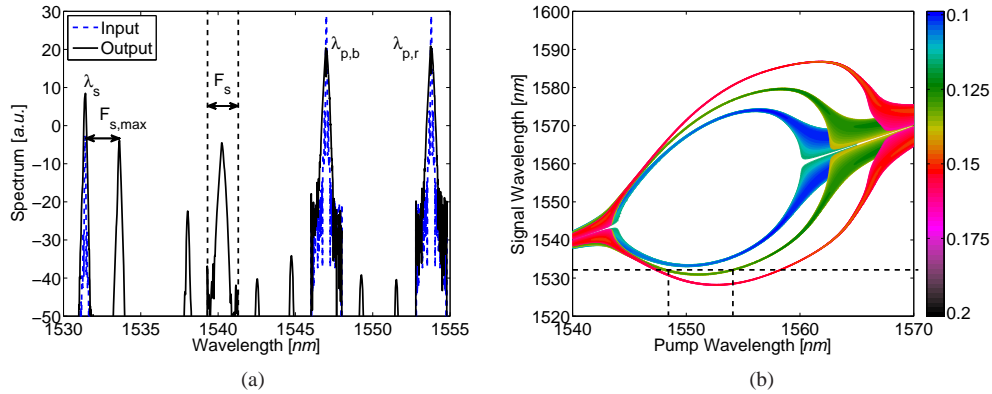

Fig. 3. (a) Input (blue curve) and output (black curve) spectra with two pumps at $\lambda_{p,b}$ and $\lambda_{p,r}$, a signal at λ_s and many high-order idlers, where the simulation sampling frequency is F_s. (b) FWM maps for the parametric gain coefficient (taken from [14]) describing where parametric gain is obtained for T/a values of 0.1, 0.125 and 0.15. The choice of the two pumps in (a) matches the FWM map of $T/a = 0.125$ (green curve with dashed lines) so that each of the pumps generates NB-OPA in the region of the signal wave.

For a choice of a blue-pump, a q value and a sampling frequency F_s, the range of possible signal wavelengths is limited by the channel separation condition: $\omega_{p,r} \leq \omega_{p,b} - 2\pi n F_s$. These

limitations are the basis for the simulations performed in sections 4-6, with different values of q.

Finally, we note that the M-SSFT algorithm loses its advantage in computation time [20] once the spectrum becomes dense (e.g. Fig. 3(a)). The number of channels increases as n increases, and also when the signal detuning decreases. Nevertheless, we maintain the use of the M-SSFT algorithm to ensure that the dispersion in nonlinear parameters is properly included. This dispersion cannot be accounted for with the conventional SSFT algorithms [19, 21].

4. Two pumps beating with amplified idlers

In this section, we address the scenario of two strong pump waves which mix in the PhC waveguides. Their wavelengths are chosen in the normal dispersion region (between the two ZDWs), so that the short-wavelength idler, generated by FWM, is phase matched with the two pumps and amplified (as described in section 2). The pulsed pump waves generate a pulsed idler. This is useful for generation of PhC waveguide based optical oscillators similar to fiber based optical parametric oscillators (FOPO) [18, 23]. This is described in the spectrum of Fig. 4(a) with the corresponding pulse profiles shown in Fig. 4(b). The asymmetry in Fig. 4(a) results from the fact that the short-wavelength idler is phase matched with the two pumps and is hence amplified while phase matching conditions for the long wavelength idler are not satisfied. Also, the losses at 1535nm are smaller than those at 1575nm and this also contributes to the asymmetry. For two identical 100ps pump pulses with profiles taken from experiments, each having a peak power of 750mW, the FWM is sufficiently efficient to yield an output idler pulse with a peak power of 133mW, about 9% of the total input power. The two pump pulses get distorted upon propagation due to a combination of linear dispersion, SPM and XPM. This distortion is similar to what is observed in optical fibers when high power pulses propagate in the normal dispersion regime [19]. The idler pulse width (about 25ps at half-power) is shorter than that of the input pulses, as in the case of NB-OPA with a single pump [14]. The pulse shortening stems from the
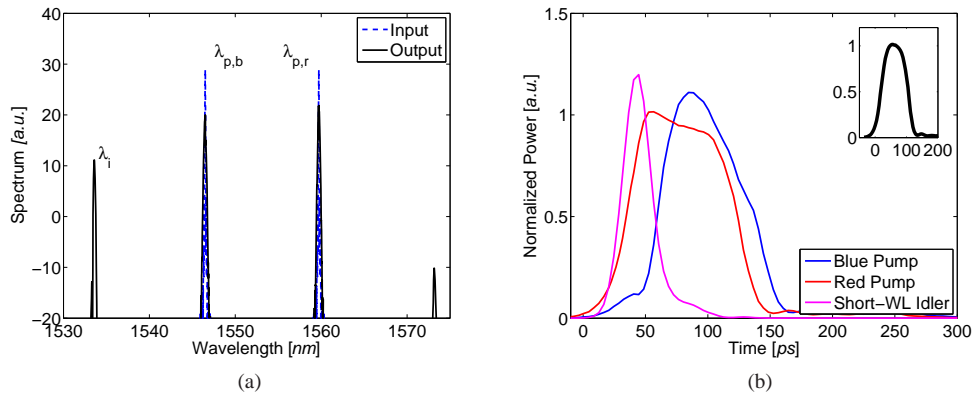

Fig. 4. Example of (a) input and Output spectra and (b) output envelope profiles of two strong pumps with FWM idlers in the engineered PhC waveguides ($T/a = 0.15$). In (a) the input (dash) spectrum belongs to two strong pumps that produce two idler waves at shorter and longer wavelengths that are added to the output (black) spectrum. In (b) the identical input profiles (shown in the inset) of both pumps get distorted while the short wavelength idler is produced with a narrower envelope.

fact that the pulse peak experiences a larger parametric gain compared to the tails.

According to the formalism described in section 3, we perform the simulations with $q = 1$, such that for every pair of desired idler and blue-pump frequencies, given by ω_i and $\omega_{p,b}$ respectively, the red-pump frequency is set by $\omega_{p,r} = 2\omega_{p,b} - \omega_i$. As mentioned before, we must account also for the evolution of the idler envelopes that are formed along the waveguide, growing or diminishing according to the overall phase matching condition for each one. With two strong pump waves that are detuned from each other by Ω_p, there could be idler waves forming as far as $2\Omega_p$ or $3\Omega_p$ away (up to the limits of high losses as in Fig. 1(b)), and the interaction between all them affects the total output power. Thus our simulations use five and six envelopes that are detuned by Ω_p from each other, each represented by a vector of less than 200 samples (with the exact numbers varying between iterations).

Figures 5(a), 5(c) and 5(e) show the ratio between the peak pulse power of the short-wavelength idler and the combined peak powers of the pumps (1.5W), as a function of the desired idler wavelength. Each figure represents a different T value, and the different curves in each figure represent different blue pump wavelengths. Conversion efficiencies of up to $-5dB$ can be obtained for an idler wavelength that ranges between $1533nm$ and $1539nm$, where in waveguides with larger T, the optimum conversion efficiency shifts to shorter wavelengths, and for a given blue-pump wavelength, the possible idler wavelength span is narrowed (similar to single pump NB-OPA [14]). In all waveguides, as the blue-pump is further detuned from the short ZDW, the optimum conversion ratio is achieved for shorter wavelengths.

As it was shown in our previous work [14], the scalability of the spectra of the propagation parameters also makes the FWM characteristics scalable when normalizing the wavelength detunings by the distance between the ZDWs:

$$\Delta_{p,b} = \frac{\lambda_{p,b} - \tilde{\lambda}_1}{\tilde{\lambda}_2 - \tilde{\lambda}_1}, \Delta_i = \frac{\lambda_i - \lambda_{p,b}}{\tilde{\lambda}_2 - \tilde{\lambda}_1}, \tag{6}$$

where $\tilde{\lambda}_1$ and $\tilde{\lambda}_2$ are the short and long ZDWs, respectively. The conversion ratio curves are plotted versus the normalized idler detuning Δ_i, and for different blue-pump detuning $\Delta_{p,b}$ in Fig. 5(b), 5(d) and 5(f). The maximum conversion is obtained for similar combinations of Δ_i and $\Delta_{p,b}$ for all T values, yet the spectra are narrower as T grows.

In light of the high conversion efficiencies for some dual-pump schemes, it is reasonable that the conversion process saturates at one point along the waveguide as the amplified idler power approaches that of the pumps. As described in section 2, both pumps transfer energy to the short-wavelength idler, yet energy is also transferred from the blue-pump to the red-pump, and so it is expected that the blue-pump power depletes faster than the red pump. This is observed when performing the simulations for different lengths of the PhC waveguide of $T/a = 0.1$. The blue-pump was set to $1545nm$ and the red pump was set so that the desired idler will be generated at either $1538.9nm$ or $1537.4nm$ (when power conversion are expected to be high and low respectively according to Fig. 5(a)). Figures 6(a) and 6(b) show, for either blue-pump, red-pump and short wavelength idler respectively, the ratio between the pulse power and the total input power (1.5W) as a function of waveguide length.

In both scenarios, the power of the red-pump reduces moderately since it both receives and transfers energy. In addition, the inherent losses of the waveguides reduces the power of all waves. The evolutions of the blue-pump and idler reflect the impact of phase matching and saturation along the waveguide. In these scenarios, the typical nonlinear length $L_{NL} = (\gamma P_p)^{-1}$, corresponding to a $750mW$ pump and a γ_{SPM} of $3\frac{1}{Wmm}$ (Fig. 1(b)), is about $0.44mm$. This fits well with the evolution of the idler power in both presented cases. Its power increases as more photons are converted from the strong pumps, however when phase matching is not satisfied, as in Fig. 6(b), power is cycled back to the pumps after a distance L_{NL}.
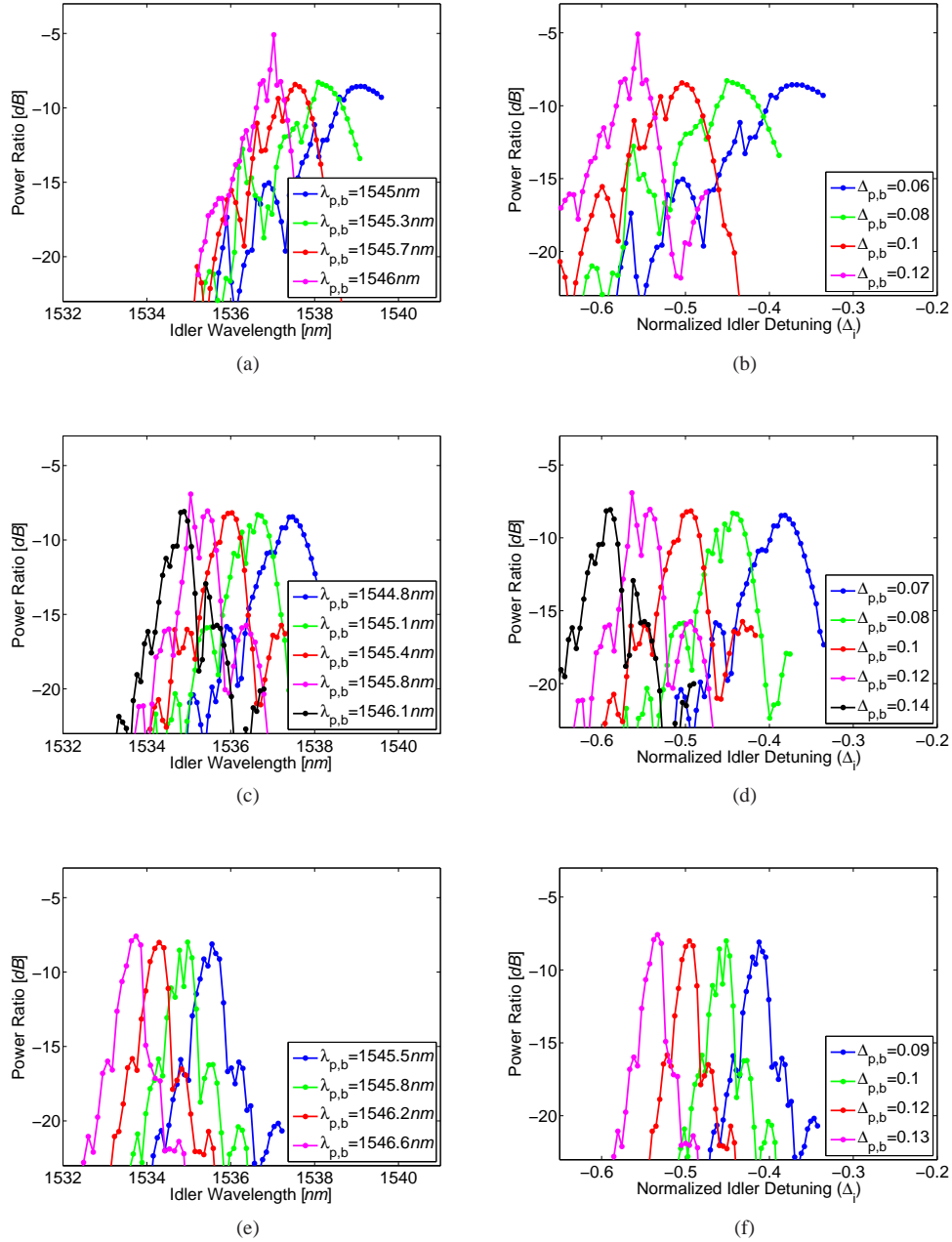
Fig. 5. Conversion ratio of the output short-wavelength idler pulse to the input pumps power in waveguides having different T/a. The ratios are plotted against an absolute or normalized wavelength scales: (a,b) $T/a = 0.1$, (c,d) $T/a = 0.125$, (e,f) $T/a = 0.15$. The different curves are plotted against desired idler wavelength, and each curve represent different blue-pump wavelength choice. As T grows, the conversion efficiency spectra become narrower.
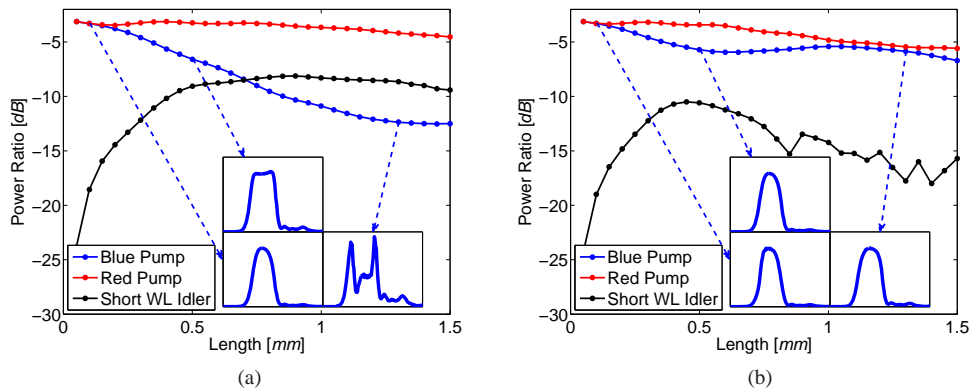
Fig. 6. The evolution of the blue-pump (blue dots) red-pump (red dots) and short-wavelength idler (black dots) along the waveguide. The vertical axis describes the ratio between the pulse power and the total input power (1.5W). The blue-pump was set to 1545nm and the red pump was set so that the desired idler will be generated at (a) 1538.9nm (with optimal phase matching) and (b) 1537.4nm (with phase miss-match). The insets show the envelope of the blue-pump at selected points along the waveguide.

When phase matching is optimal as in Fig. 6(a), the blue-pump power is depleted while the idler gains more power. Saturation is reached after 0.7mm when the idler reaches the same power as the blue-pump. The blue-pump is strongly coupled to the red-pump and to the idler and consequently, its envelope profile is distorted due to both linear dispersion and the nonlinear processes, as can be seen in the insets in Fig. 6(a).

5. Amplification by two pumps

Next we turn to the case of parametric amplification of a signal pulse using two strong pulsed pump waves spectrally placed in the normal dispersion region. The input profiles of all the waves is identical, and given by the measured profile used in section 4, while the input peak powers of the signal and the pumps are 0.5mW and 750mW respectively. An exemplary spectrum of the waves in this configuration was already presented in Fig. 3(a) featuring the pumps and signal spectra together with the spectra of the numerous idlers generated by multiple FWM interactions.

Figures 7(a)-7(c) show the gain of the signal pulse as a function of its wavelength. The different figures represent different T values with and each curve representing a different choice of blue-pump wavelength and a q value. More configurations of dual-pump schemes can be chosen with different q values, yielding different optimum efficiencies at different signal wavelengths. The gain curves in these cases are formed with the maximum signal-pump detuning (similar to the detuning range with a single pump in [14]). Of course the maximum gain for these signal wavelengths is larger than the attainable gain with a single pump since the total power is higher. Furthermore, the dependence on the asymmetric shift T is the same, as the gain spectra narrow when T increases.

Note that the gain spectra are no more than 1nm wide. Thus according to Eq. (5), given a choice of q and pump wavelength $\lambda_{p,b}$, the wavelength of the appropriate red-pump $\lambda_{p,r}$, shifts by a small amount as well (assuming that $\frac{\lambda_{p,r}}{\lambda_s} \frac{\omega_s}{\omega_{p,r}} \sim 1$):
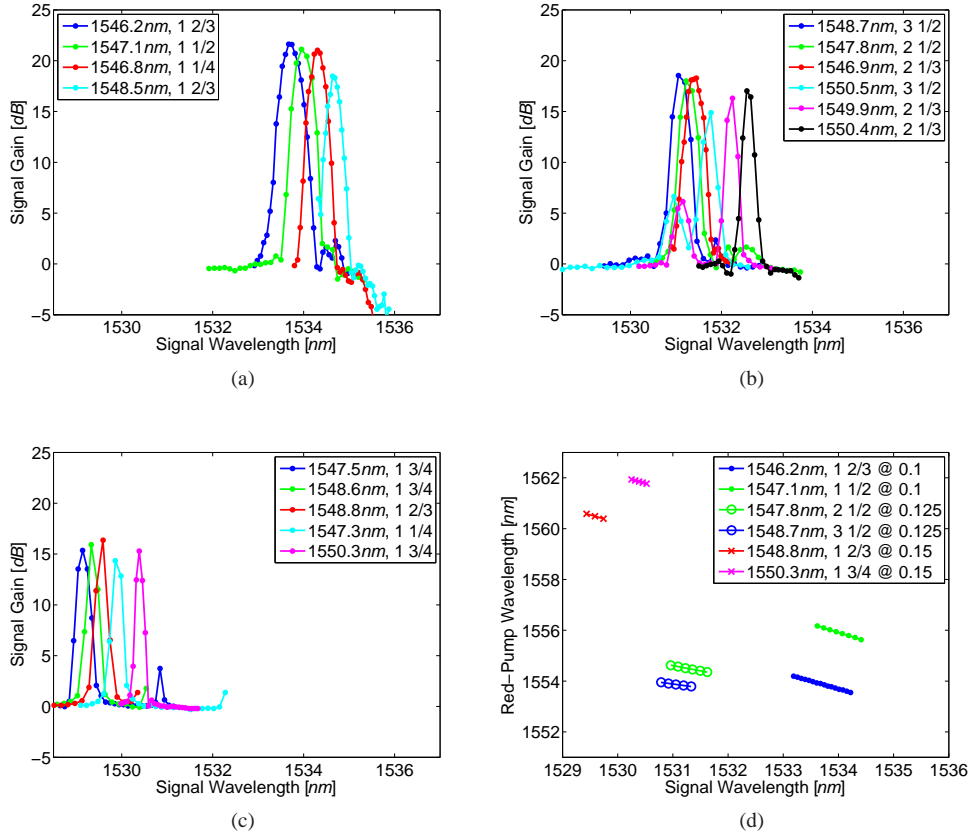
Fig. 7. Gain spectra for different dual-pump schemes (with $100ps$ pulses) in engineered PhC waveguides with (a) $T/a = 0.1$, (b) $T/a = 0.125$ and (c) $T/a = 0.15$. The blue-pump wavelength $\lambda_{p,b}$ and the q values are stated in the legends. (d) Calculated red-pump wavelength $\lambda_{p,r}$ for a few dual-pump schemes taken from (a), (b) and (c) in regions where the gain is larger than $3dB$. $\lambda_{p,r}$ changes by no more than $1nm$ and can be considered fixed. Here the legend is formatted as $\lambda_{p,b}, q @ T/a$.

$$\Delta\lambda_{p,r} \cong \frac{1}{q}\Delta\lambda_s. \tag{7}$$

These results are equivalent to a fixed-wavelength dual-pump scheme where the signal wavelength is tuned. We plot in Fig. 7(d) the value of $\lambda_{p,r}$ as function of λ_s for different dual-pump schemes.

When comparing to simulation performed with a single pump, we note that the gain spectrum of the blue-pump together with that of the matching red-pump (for the same signal wavelength) do not add-up to the gain spectra shown in 7(a)-7(c). This is attributed to the contributions of XPM between the pumps and also due to the interaction between many idler waves that are generated along the waveguide and do not exist in the single pump case.

6. Amplification of high bit-rate data streams

In addition to enhancing the parametric gain, we examine also amplification and distortion of high bit-rate data streams. We compare NB-OPAs with a single $750mW$ pump to the dual-pump schemes in which each pump is $375mW$ (equal total input power). In each of these scenarios, the signal is comprised of a $40Gbps$ NRZ data stream made up of 1024 pulses having a peak power of $0.5mW$, while the pumps are CW. We chose the PhC waveguide with $T/a = 0.15$, and performed several simulations for each scenario using different pump wavelengths (and $q = 1^1/_2$ for the dual-pump scheme) as well as different signal wavelengths.
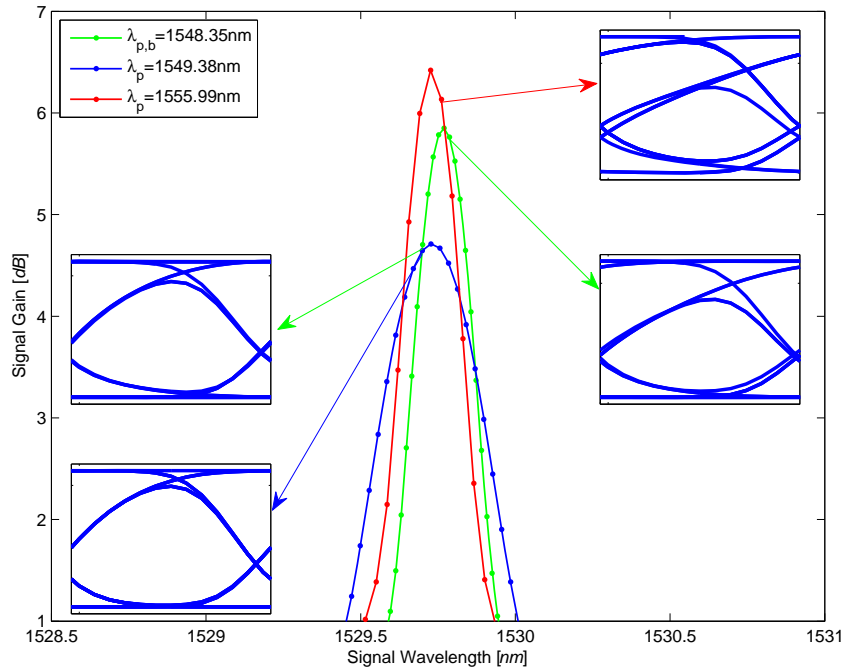

Fig. 8. Curves of the average signal gain as a function of the NRZ signal carrier wavelength for the two OPA types: a dual-pump scheme with $375mW$ each (green curve) and a single pump with $750mW$ (blue and red curves). The calculations are for an engineered PhC waveguide with $T/a = 0.15$. The insets depict the eye diagrams for output signals around $1529.7nm$ at different OPA configurations.

We computed the average gain experienced by the signal and also examined the eye diagram at the output. Fig. 8 shows the gain for the single pump OPAs (blue and red curves) and a dual-pump scheme (green curve), as a function of the signal carrier wavelength. The legend states the blue-pump wavelength of the dual-pump case (the red-pump wavelength is chosen, as before, to match the signal wavelength and the q value), and the wavelengths of the single pump amplifiers. Since the spectral width of the signal is comparable to the narrow band gain

bandwidth, it is necessary to characterize the amplifier by an average gain. Each point in Fig. 8 represents such an average gain value which is the ratio of the output pulse train energy (determined by the gain spectrum and the spectral content of the $40Gbps$ signal) and the energy of the input signal.

The average gain (Fig. 8) contains no information about any distortions experienced by the amplified data stream. To that end, we calculate the output eye diagram for each pump and signal carrier wavelength. Examples are given by the insets in Fig. 8 for which it appears that as the attainable gain rises, the eye-opening reduces since a single $25ps$ pulse does not experience the maximum possible gain that is attainable from the $750mW$ pump power. This is attributed to the $40Gbps$ signal bandwidth being wider than the parametric gain spectrum. We examine the eye opening of each output signal, compare it to the eye opening value of the input signal (an ideal reference signal) and calculate the eye opening ratio, shown in Fig. 9(a) as a function of signal carrier wavelength. Each value in Fig. 9(a) matches an appropriate gain value in Fig. 8 for the same carrier wavelength and same single or dual-pump OPA. It is clear that as the signal wavelength is shifted to where maximum gain is obtained, the eye diagram closes since short sections of the data stream are not fully amplified. In the case of a single pump OPA, a larger eye opening is obtained for pump positioned close to the short ZDW as compared with those positioned close to the long ZDW. This happens since the longer wavelength pump is positioned deep in the normal dispersion region, where phase matching (and hence gain) occurs in a narrower region compared with the phase matching region due to the shorter wavelength pump.
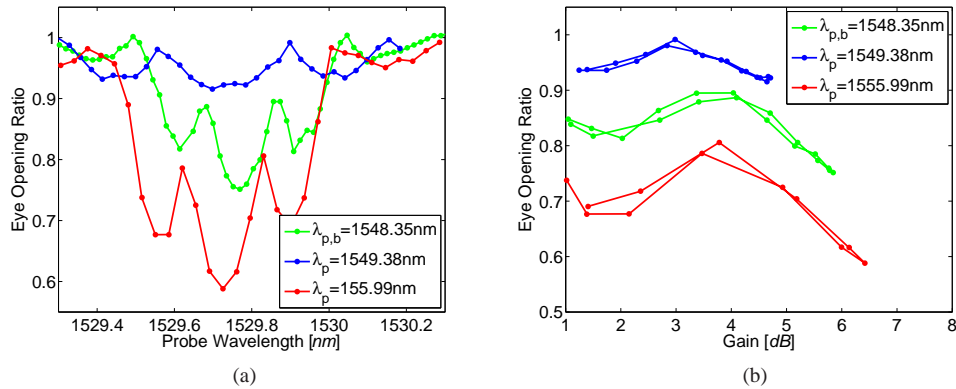

(a) (b)

Fig. 9. (a) Eye opening ratio of the signal as a function of signal wavelength for the two OPA types: a dual-pump scheme with $375mW$ each (green curves) and a single pump with $750mW$ (blue and red curves). The calculations are done for simulations performed in an engineered PhC waveguide with $T/a = 0.15$. (b) Curves of the eye opening ratio matching the average signal gain. These curves show that signal output is cleaner after the dual-pump OPA given the same gain level as a single pump OPA, for gain above $5dB$.

In order to better understand the trade-off between attainable gain and signal distortion (eye opening), we plot in Fig. 9(b) the eye opening ratio against the corresponding average signal gain (of the same signal wavelength and the same pump configurations). With a fix input pump power one can obtain a certain gain and eye opening level. If a low gain value suffices, a single pump can be used, preferably placed close to the short ZDW (the blue curve). If a larger gain is needed, for the same total input power, the pump should be positioned at a proper wavelength

close to the long ZDW such that phase matching is achieved for the same signal wavelength (the red curve), however this comes at the expense of the eye opening. A better option is to use two pump waves, at proper wavelengths such that phase matching is obtained at the desired signal wavelength (the green curve). Larger gain can be obtained compared with the single pump amplifier, yet the signal suffers less distortion. An optimization is possible by which the power is divided among the two pumps. We note that an improvements of 10% can be achieved with even power distribution.

7. Conclusion

To conclude, we have presented results obtained by numerical simulations of parametric amplification in a dispersion engineered PhC waveguide which exhibit two ZDWs. In the spectral vicinity of each ZDW, we place a pump wave and together they enhance the NB-OPA. The M-SSFT algorithm [20] was implemented in the simulations since it allows for the incorporation of dispersive nonlinear propagation parameters and losses, making it most suitable for calculating NB-OPA in such complex waveguides.

The scenario of amplified idler waves was shown first, when two pump pulses are launched together and the short-wavelength idler generated by FWM on the blue-pump side is amplified by the enhanced parametric process. Power conversion of up to $-5dB$ is achieved when launching two $750mW$ pumps. This could be used for a PhC based optical oscillator, similar to those implemented in optical fibers [18]. Simulations of an amplified signal were presented as well showing enhanced gain compared with NB-OPA by a single pump. In both scenarios we examined the effect of the asymmetric shift parameter T that controls the propagation parameters of the engineered PhC waveguide. As with the case of a single pump (shown in [14]), by increasing T we narrow the effective range of signal wavelengths for which parametric gain is attainable for a given dual-pump scheme.

Amplification and distortion of data signals were used together to compare single and dual-pump amplifiers. The dispersion engineered PhC waveguides enables to trade off gain and distortion by spectrally positioning the pumps in the normal dispersion regime close to either the short or the long ZDW. Moreover, with a dual-pump scheme, it is possible to distribute the power between the two pumps (positioned appropriately in the vicinity of each ZDW) so as to obtain a larger gain with a reduced signal distortion. This degree of freedom is an advantage of the dispersion engineered PhC over conventional $W1$ waveguides (where the dispersion is only anomalous) and over fibers which exhibit but one ZDW.